Int. J. Heat Mass Transfer. Vol. 25, No. 2, pp. 277–284, 1982
Printed in Great Britain

0017-9310/82/020277-08 $03.00/0

NATURAL CONVECTION IN A VERTICAL STACK OF INCLINED PARALLELOGRAMMIC CAVITIES

KYUNG CHO CHUNG
GTE Laboratories Inc., Waltham, MA 02154, U.S.A.

and

LLOYD M. TREFETHEN
Department of Mechanical Engineering, Tufts University, Medford, MA 02155, U.S.A.

(*Received* 12 *January* 1981 *and in revised form* 15 *July* 1981)

Abstract—Natural convection within a vertical stack of long, inclined parallelogrammic cavities is examined numerically. An explicit, finite difference scheme for 2-dim. flow is formulated along with appropriate boundary conditions. Nusselt numbers are computed for several geometries, Prandtl numbers, Grashof numbers, and conductances between cavities. These analytical results provide a basis for comparison with data that have been obtained with 'oneway' heat walls. The procedure also provides a basis for estimating the potential of such asymmetrical insulating structures; one conclusion is that conduction between cavities considerably reduces the asymmetry attainable in overall Nusselt number.

NOMENCLATURE

b, thickness of partition wall;
c_p, specific heat at constant pressure;
D, height of parallelogrammic cavity;
g, gravitational acceleration;
Gr, Grashof number, $D^4 g\beta(T_h - T_c)/(Ly^2)$;
k_b, thermal conductivity of partition wall;
k_f, thermal conductivity of fluid;
l, dimensionless length of parallelogram, L/D;
L, length of parallelogram;
n, coordinate normal to $\tilde{y}$-axis;
Nu, Nusselt number as defined by eqn. (24);
p, pressure;
Pr, Prandtl number, $c_p\mu/k_f$;
$\dot{q}$, local heat flux density;
$\dot{Q}$, total heat flux defined by eqn. (21);
Ra, Rayleigh number, $Pr \times Gr$;
Rc, ratio of conductances, $(k_b/b)/(k_f/D)$;
t, time;
T, temperature;
u,v, velocity in x- and y-direction respectively;
V, velocity in the direction normal to $x = l/2$;
x,y, rectangular coordinates;
$x,\tilde{y}$, parallelogrammic coordinates.

Greek symbols

α, angle of inclination of partition wall;
β, thermal expansion coefficient of fluid;
Δt, time increment;
$\Delta x, \Delta y, \Delta\tilde{y}$, grid space in x-, y- and $\tilde{y}$-direction respectively;
ζ, vorticity function, $\partial u/\partial y - \partial v/\partial x$
γ, ratio of Nusselt numbers, $Nu^{(+)}/Nu^{(-)}$;
η, quantity defined by eqn. (23);
μ, dynamic viscosity;
ν, kinematic viscosity;
ρ, fluid density;
ψ, stream function;
ω, relaxation factor.

Subscripts

B, boundary wall;
cd, conduction only;
cdv, conduction plus convection;
h,c,m, hot, cold and medium temperature respectively;
i,j, grid number in $\tilde{y}$- and x-direction respectively;
M,N, number of basic grids in x- and $\tilde{y}$-direction respectively.

Superscripts

$*$ new value of function after one step of time increment;
$(+),(-)$ value when α is positive and negative respectively.

INTRODUCTION

THERE is at the present time much interest in efficient use of energy. An insulating material that conducts heat one way but not the other would obviously be widely useful. A vertical stack of inclined cavities possesses such an asymmetrical property, to a limited degree. This paper presents an analysis of such a stack of cavities, in which a fluid acts as a convector of thermal energy.

Steady 2-dim. natural convection in rectangular enclosures with isothermal vertical walls has been extensively studied during the past two decades. Among the investigators, Batchelor [1] and Elder [2]

dealt analytically with long, vertical geometries, and Eckert and Carlson [3] investigated the problem experimentally. Wilkes and Churchill [4], de Vahl Davis [5], and Quon [6] examined short, rectangular enclosures numerically.

Convection in inclined rectangular cavities has been investigated numerically by Ozoe, Sayama and Churchill [7] and Catton, Ayyasawamy and Clever [8]. Dropkin and Somerscales [9], and Arnold, Catton and Edwards [10] reported experimental data for inclined rectangular geometries.

The studies listed above have two characteristic geometric features: flows are 2-dim. in rectangular cavities; and, only single cavities are considered. Trefethen [11] reports on a series of experiments with water in long, circular, inclined tubes. The ratio of length to diameter was large, varying from 50 to 500. In some, one end of the tube was heated and the other cooled while the tube was at various degrees of inclination. In others, salt instead of heat was diffused axially, eliminating thermal insulation as an experimental problem. The experimental data [11, 12] show the ratio of Nusselt numbers for opposite angles of inclination varying with angle and Rayleigh number. Values of the ratio reached as high as 10^6.

Such high ratios are definitely not obtained along short, stacked cavities. In a recent series of experiments [12] with air and with water in vertical stacks of cavities resembling Venetian blinds, the Nusselt number ratios obtained were of order 10, with a maximum value of 17. The results of the present analysis (which were partially reported in [12]) explain why. The end effects of short cavities, and finite conduction between cavities, act markedly to reduce the natural convection asymmetry induced by opposite inclinations of the gravity vector.

FORMULATION OF THE PROBLEM

1. *Governing equations*

The physical system consists of a Newtonian fluid in a cavity which forms a parallelogram with two vertical walls and two, arbitrarily inclined, parallel partition walls, as shown in Fig. 1. To formulate the problem it was assumed that: (a) the fluid motion and temperature functions are 2-dim.; (b) the fluid is viscous and incompressible; (c) frictional heating is neglible; (d) the difference between the two constant temperatures on the vertical walls is small compared with $1/\beta$, and (e) fluid properties are constant except for density variation with temperature. Thus, four governing equations (two momentum, one energy and one continuity) are at hand:

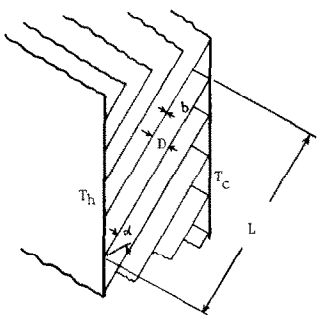

FIG. 1. Geometry of a vertical stack of inclined cavities with isothermal walls.

$$\frac{\partial u}{\partial t}+u\frac{\partial u}{\partial x}+v\frac{\partial u}{\partial y}=-\frac{1}{\rho}\frac{\partial p}{\partial x}+g\beta(T-T_m)\sin\alpha+\nu\nabla^2 u, \quad (1)$$

$$\frac{\partial v}{\partial t}+u\frac{\partial v}{\partial x}+v\frac{\partial v}{\partial y}=-\frac{1}{\rho}\frac{\partial p}{\partial y}+g\beta(T-T_m)\cos\alpha+\nu\nabla^2 v, \quad (2)$$

$$\frac{\partial T}{\partial t}+u\frac{\partial T}{\partial x}+v\frac{\partial T}{\partial y}=\frac{k_f}{\rho c_p}\nabla^2 T, \quad (3)$$

and

$$\frac{\partial u}{\partial x}+\frac{\partial v}{\partial y}=0 \quad (4)$$

where

$$\nabla^2\equiv\frac{\partial^2}{\partial x^2}+\frac{\partial^2}{\partial y^2}.$$

All variables in the above equations are made dimensionless by substituting the following variables into equations (1–4):

$$\left.\begin{aligned} x'=x/D,\quad y'=y/D,\quad u'=uD/\nu,\\ v'=vD/\nu,\quad t'=t\nu/D^2,\quad p'=pD/\rho\nu^2,\\ T'=(T-T_m)/(T_h-T_m).\end{aligned}\right\} \quad (5)$$

Dropping the primes, eliminating pressure terms between the first two equations, and employing the stream and vorticity functions leads to:

$$\frac{\partial\zeta}{\partial t}=-u\frac{\partial\zeta}{\partial x}-v\frac{\partial\zeta}{\partial y}-\frac{1}{2}Gr(L/D)\times\left[\frac{\partial T}{\partial y}\sin\alpha-\frac{\partial T}{\partial x}\cos\alpha\right]+\nabla^2\zeta, \quad (6)$$

$$\frac{\partial T}{\partial t}=-u\frac{\partial T}{\partial x}-v\frac{\partial T}{\partial y}+\frac{1}{Pr}\nabla^2 T, \quad (7)$$

$$\zeta=-\nabla^2\psi, \quad (8)$$

$$u=\frac{\partial\psi}{\partial y},\quad v=-\frac{\partial\psi}{\partial x}. \quad (9)$$

In order to facilitate the application of boundary conditions, which will be specified later, to the governing equations, the x–y coordinates system was transformed to x–$\tilde{y}$ coordinates, which can be called 'skewed' or 'parallelogrammic' coordinates as shown in Fig. 2. Between the two coordinate systems, the following relationships of differential operators hold [13]:

$$\left(\frac{\partial}{\partial y}\right)^n_{x-y\,\text{coord.}}=\left(\frac{1}{\cos\alpha}\frac{\partial}{\partial\tilde{y}}-\tan\alpha\frac{\partial}{\partial x}\right)^n_{x-\tilde{y}\,\text{coord}}, \quad (10a)$$

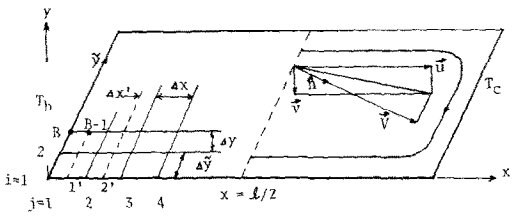

FIG. 2. Finite grid system and velocity component, V, normal to the plane $x = l/2$.

$$\left(\frac{\partial}{\partial x}\right)^n_{x-y\,\text{coord}} = \left(\frac{\partial}{\partial x}\right)^n_{x-\tilde{y}\,\text{coord}} \tag{10b}$$

where $n = 1$ or 2 for the present problem. Transforming equations (6–9) into the new coordinate system yields:

$$\frac{\partial \zeta}{\partial t} = \frac{1}{\cos\alpha}\left(\frac{\partial \psi}{\partial x}\frac{\partial \zeta}{\partial \tilde{y}} - \frac{\partial \psi}{\partial \tilde{y}}\frac{\partial \zeta}{\partial x}\right) - \frac{1}{2}l\cdot Gr\left(\tan\alpha\frac{\partial T}{\partial \tilde{y}} - \frac{1}{\cos\alpha}\frac{\partial T}{\partial x}\right) + \frac{1}{\cos^2\alpha}\left(\frac{\partial^2\zeta}{\partial x^2} - 2\sin\alpha\frac{\partial^2\zeta}{\partial x\partial\tilde{y}} + \frac{\partial^2\zeta}{\partial\tilde{y}^2}\right) \tag{11}$$

$$\frac{\partial T}{\partial t} = \frac{1}{\cos\alpha}\left(\frac{\partial \psi}{\partial x}\frac{\partial T}{\partial \tilde{y}} - \frac{\partial \psi}{\partial \tilde{y}}\frac{\partial T}{\partial x}\right) + \frac{1}{Pr\cos^2\alpha}\left(\frac{\partial^2 T}{\partial x^2} - 2\sin\alpha\frac{\partial^2 T}{\partial x\partial\tilde{y}} + \frac{\partial^2 T}{\partial\tilde{y}^2}\right) \tag{12}$$

and

$$\zeta = -\frac{1}{\cos^2\alpha}\left(\frac{\partial^2\psi}{\partial x^2} - 2\sin\alpha\frac{\partial^2\psi}{\partial x\partial\tilde{y}} + \frac{\partial^2\psi}{\partial\tilde{y}^2}\right) \tag{13}$$

2. Initial and boundary conditions

Initially, the fluid in the cavity is stationary with a uniform temperature, an average value of the two wall temperatures:

$$\zeta = \psi = T = 0 \quad \text{everywhere at } t = 0. \tag{14}$$

The non-slip condition and global continuity require:

$$\psi = \frac{\partial\psi}{\partial x} = \frac{\partial\psi}{\partial\tilde{y}} = 0 \quad \text{on boundary walls.} \tag{15}$$

And for temperatures on the isothermal walls:

$$T(x = 0) = 1 \text{ and } T(x = l) = -1. \tag{16}$$

The iteration technique of the implicit boundary conditions for the temperature on the inclined partition walls and vorticity on the boundary walls will be shown later.

3. Finite difference approximations

Equations (11–13) represent the vorticity, energy, and stream-function equations in the x–$\tilde{y}$ coordinates plane. To solve them along with the boundary conditions, an explicit form of finite-difference approximation was formulated. Figure 2 shows a finite grid system, where the problem domain is divided into $M \times N$ small parallelogrammic grids with dimensions $\Delta x \times \Delta\tilde{y}$, where $\Delta x = l/M$ and $\Delta\tilde{y} = 1/(N\cdot\cos\alpha)$.

At every grid point of the inside domain, the governing equations approximated by finite difference forms should be satisfied at every time step. Time derivatives are approximated by forward differences, while spatial derivatives by central differences making equations (11) and (12) into time-marching forms for vorticity and temperature solutions respectively. Equation (13) is approximated into a relaxation formula for stream function:

$$\zeta^*_{i,j} = \zeta_{i,j} + \Delta t \times F_1(\psi,\zeta,T), \tag{17}$$

$$T^*_{i,j} = T_{i,j} + \Delta t \times F_2(\psi,T), \tag{18}$$

$$(\psi_{i,j})_{\text{new}} = \psi_{i,j} + \omega \times [F_3(\psi,\zeta) - \psi_{i,j}], \tag{19}$$

where F_1, F_2 and F_3 are functions of computed values of ψ, ζ and T.

In order to minimize inaccuracy of the solution near the isothermal walls, where velocity and temperature gradients are high, subdivisions were made between $j = 1$ and 3 in Fig. 2. Details are shown in Table 1.

NUMERICAL PROCEDURE

1. Computational economization

Numerical integration of the finite difference equations leading to a steady solution was carried out using a time increment, Δt, for equations (17) and (18), and a relaxation factor, ω, for equation (19) with static boundary conditions (15) and (16) and dynamic boundary conditions which will be specified later. Computing time was reduced considerably without sacrificing accuracy of the solution by taking advantage of the following:

(a) *Characteristics of unknown functions.* If a function $f(x, y)$ remains the same when x and y coordinates change their signs, the function is called an even function, but, if its sign only changes, it is called an odd function in the x–y plane.

In the present problem, let the origin of x–$\tilde{y}$ coordinates be assumed to be at the center of the cavity, which is symmetric with respect to this point. Inspection of equations (11), (12) and (13), boundary conditions (15) and (16), and implicit boundary conditions (28), (29) and (32), indicates that the vorticity, ζ, and stream function, ψ, can be treated as even functions while the temperature field as an odd function throughout the transient and steady flow regimes because initial conditions also meet the same characteristics of the functions. Therefore, in the present time integration, only half of the cavity is required for computation for a complete solution. A set of new boundary conditions at $x = l/2 + \Delta x$, which

Table 1. Finite grid mesh data

L/D	N	M	Δy	Δx	$\Delta x'$
5	10	20	0.1	0.25	$\Delta x/2$
10	10	26	0.1	0.3846	$\Delta x/3$
20	10	40	0.1	0.5	$\Delta x/4$

replace those at $x = l$, can be computed in step-by-step manner:

$$\left.\begin{aligned}(\zeta_{i,M/2+2})_{\text{new B.C.}} &= \zeta_{N+2-i,M/2}\\ (\psi_{i,M/2+2})_{\text{new B.C.}} &= \psi_{N+2-i,M/2}\\ (T_{i,M/2+2})_{\text{new B.C.}} &= -T_{N+2-i,M/2}\end{aligned}\right\} \quad (20)$$

where $i = 1, 2, 3 \ldots, N + 1$.

(b) *Computation of heat flux along $x = l/2$.* If a calculation of overall heat flux between the two isothermal walls is made along one of the walls, its accuracy would heavily depend upon the grid size near the wall [13]. In order to calculate the heat flux accurately without having to have very small size of grid near the isothermal walls, the total heat flux was computed at $x = l/2$. The total heat flux per unit thickness along $x = l/2$ (Fig. 2) is:

$$\dot{Q}_{\text{cdv}} = k_{\text{f}}(T_{\text{h}} - T_{\text{m}}) \times \left[\int_0^{1/\cos\alpha} \left(PrVT - \frac{\partial T}{\partial n}\right)_{x=l/2} \mathrm{d}\tilde{y}\right]_{\text{cdv}} \quad (21)$$

where $k_{\text{f}}(T_{\text{h}} - T_{\text{m}})$ is dimensional. The first term in the integral represents the heat flux by convection and the second by conduction. If the heat flux is only by conduction then

$$\dot{Q}_{\text{cd}} = k_{\text{f}}(T_{\text{h}} - T_{\text{m}})\eta \quad (22)$$

where

$$\eta = -\left[\int_0^{1/\cos\alpha} \left(\frac{\partial T}{\partial n}\right)_{x=l/2} \mathrm{d}\tilde{y}\right]_{\text{cd}}. \quad (23)$$

The Nusselt number is defined as

$$Nu = \frac{1}{\eta}\left[\int_0^{1/\cos\alpha} \left(Pr\,VT - \frac{\partial T}{\partial n}\right)_{x=l/2} \mathrm{d}\tilde{y}\right]_{\text{cdv}}. \quad (24)$$

3. *Computation of implicit boundary conditions*

(a) *Temperature on the tilted partition wall.* The thickness, b, of the partition wall is assumed small such that heat conduction along the wall is negligible. Heat flux density crossing the partition wall is

$$q_j = -k_{\text{f}}\left(\frac{\partial T}{\partial y}\right)_{1,j} = -k_{\text{f}}\left(\frac{\partial T}{\partial y}\right)_{N+1,j} \simeq -k_{\text{b}}(T_{1,j} - T_{N+1,j})/b. \quad (25)$$

From equations (10) and (25) we have

$$\left(\frac{1}{\cos\alpha}\frac{\partial T}{\partial \tilde{y}} - \tan\alpha\frac{\partial T}{\partial x}\right)_{1,j \text{ or } N+1,j} = (k_{\text{b}}/k_{\text{f}})(T_{1,j} - T_{N+1,j})/b. \quad (26)$$

With the use of the Taylor series expansion, the temperature gradient at the bottom partition wall is approximated by

$$\left(\frac{\partial T}{\partial \tilde{y}}\right)_{1,j} \simeq \left(\frac{\partial T}{\partial \tilde{y}}\right)_{2,j} - \Delta\tilde{y}\left(\frac{\partial^2 T}{\partial \tilde{y}^2}\right)_{2,j} \simeq (-3T_{1,j} + 4T_{2,j} - T_{3,j})/2\Delta\tilde{y}. \quad (27)$$

This approximation is identical to fitting a second degree polynomial and taking the first derivative. Using expressions (25–27), the iteration formula for the bottom wall temperatures, $T_{1,j}$, is obtained:

$$T_{1,j} = [B_1 T_{N+1,j} + 4T_{2,j} - T_{3,j} - B_2(T_{1,j+1} - T_{1,j-1})]/B_3. \quad (28)$$

Similarly, for the top wall temperatures we have

$$T_{N+1,j} = [B_1 T_{1,j} + 4T_{N,j} - T_{N-1,j} + B_2(T_{N+1,j+1} - T_{N+1,j-1})]/B_3. \quad (29)$$

B_1, B_2 and B_3 in the above two equations are constant coefficients containing Rc, ratio of conductances.

(b) *Vorticity on the boundary walls.* The necessity of vorticity boundary condition calculation arises due to the elimination of pressure terms in equations (1) and (2). Integration of vorticity on the boundary walls should be done at every time step utilizing the known stream functions and vorticity values of the preceding time step.

Taking terms up to the third order in the Taylor series expansion and using boundary condition (14), we can approximate ψ_{B-1} at point B − 1 (Fig. 2) as:

$$\psi_{B-1} \simeq \sum_{m=1}^{3} \frac{1}{m!}(\Delta x)^m \left[\left(\cos\alpha\frac{\partial}{\partial n} + \sin\alpha\frac{\partial}{\partial \tilde{y}}\right)^m \psi\right]_{\text{B}} \quad (30)$$

Considering the non-slip conditions (15) and another relationship $\zeta_{\text{B}} = -(\partial^2\psi/\partial n^2)_{\text{B}}$, we obtain:

$$\psi_{B-1} \simeq -\frac{1}{2}\left[\zeta_{\text{B}}(\Delta x\cos\alpha)^2 + \frac{1}{3}\left(\frac{\partial\zeta}{\partial n}\right)_{\text{B}} \times (\Delta x\cos\alpha)^3 + \left(\frac{\partial\zeta}{\partial\tilde{y}}\right)_{\text{B}} \Delta x^3\cos^2\alpha\sin\alpha\right]. \quad (31)$$

The final iterative forms of ζ_{B} are:

$$\left.\begin{aligned}\zeta_{\text{B}} &= B_4\psi_{B-1} + B_5\zeta_{B-1} + B_5\left(\frac{\partial\zeta}{\partial\tilde{y}}\right)_{\text{B}} \quad \text{at } x = 0\\ \zeta_{\text{B}} &= B_7\psi_{B-1} + B_8\zeta_{B-1} + B_9\left(\frac{\partial\zeta}{\partial x}\right)_{\text{B}} \quad \text{at } y = 0\\ \zeta_{\text{B}} &= B_7\psi_{B-1} + B_8\zeta_{B-1} - B_9\left(\frac{\partial\zeta}{\partial x}\right)_{\text{B}} \quad \text{at } y = 1.\end{aligned}\right\} \quad (32)$$

where B_4–B_9 are constant coefficients. The terms $(\partial\zeta/\partial\tilde{y})_{\text{B}}$ and $(\partial\zeta/\partial x)_{\text{B}}$ in the above equations are approximated by central differences utilizing ζ_{B} values of the previous time step.

RESULTS AND DISCUSSION

The numerical solution in terms of temperature, T, vorticity, ζ, stream function, ψ, and the Nusselt number, Nu, is a function of several input parameters. The functional relationship of the solution function, f, is

$$f = f(L/D, \alpha, Pr, Gr, Rc) \text{ or } f(L/D, \alpha, Pr, Ra, Rc). \quad (33)$$

The inclusion of Rc is necessary. It determines the degree to which two neighboring cavities are thermally

coupled in equations (28) and (29). When $Rc = 0$, the partition walls are adiabatic.

Due to the large number of controlling parameters, the number of values for each parameters was kept small. Those taken were:

$$L/D = 5,\ 10,\ 20,$$
$$\alpha = 0,\ \pm 20,\ \pm 40,\ \pm 50,$$
$$Pr = 0.72,\ 4,\ 20,$$
$$Gr = 2000,\ 5000,\ 10\,000,$$
$$Rc = 0,\ 1,\ 10,\ 100.$$

Computation is started with the initial conditions (14), and boundary conditions (15) and (16). The implicit conditions (28), (29) and (32) are subsequently used. Since the steady solution rather than the transient is of the primary interest in this analysis, in most cases the data for the previously computed steady solution of a similar case were used for the initial state. It was confirmed by a few trial runs that the steady state solution is unique no matter what initial conditions are used. Time increments: 0.002 and 0.001 s were used throughout the entire computation. For cases of negative inclination (stably stratified fluid) the computing time took longer than for the opposite positively inclined cases.

The Nusselt number is computed using equation (24) at $x = l/2$. The denominator η should be computed in the absence of convection. These values were reported by Chung and Astill [13], and a part of them are tabulated in Table 2.

Computed Nusselt numbers for several values of L/D, Rc, α, Pr and Gr are shown in Table 3. $Pr = 0.72$ and 4.0 were selected for air and water respectively. In Fig. 3 the Nusselt numbers and their ratio γ are presented for several values of Rc and α.

With adiabatic partition walls, the Nusselt numbers were extreme: the minimum and maximum at negative and positive angles of inclination respectively. The effect of finite wall conductance, Rc, is to increase Nu at negative inclinations and reduce Nu at positive inclinations. Consequently, the ratio of Nusselt numbers, γ, decreases with the increased Rc.

The Nusselt number tends to decrease at angles beyond certain values, approximately $+25°$. However, a similar Nusselt number does not necessarily mean less heat transfer between two isothermal walls because of the presence of varying η in equation (24).

Larger magnitudes of Nu and γ can be obtained, as indicated in the figures, with smaller Rc and larger Ra. The aspect ratio, L/D, also is a dominant factor. Comparison of Nu data between the second ($L/D = 10$, $Ra = 7200$) and the fourth ($L/D = 20$, $Ra = 3600$) group of data in Table 3 (groups that would have the same Grashof number 10^5 if D^3 is used instead of D^4/L in its definition) shows that Nu values for $L/D = 20$ are as much as 85% larger than the corresponding values of $L/D = 10$.

Isotherms and normalized streamlines of steady solutions for $L/D = 10$, $Pr = 0.72$ and $Gr = 2000$ are shown in Figs. 4 and 5 for several values of Rc and α. For the positive α there is one eddy, stationed at the center of the cavity, while for $\alpha \leq 0$ there are two eddies, one near each isothermal wall. The effect of Rc is marked. Heat flux across the partition walls enhances the convective heat transfer between the two isothermal walls when the inclination of the cavity is negative. On the other hand, it hinders the heat transfer considerably for positive angles of inclination. The density of isotherms near the isothermal walls, and the magnitude of the maximum stream functions, are strongly influenced by Rc values, as can be seen in these figures.

Figure 6 shows relative magnitudes of heat flux crossing the partition wall for $\alpha = +40$, 0, and $-40°$ with $Rc = 10$. Since the hotter fluid tends to occupy the upper region of the cavity, the heat flux is almost everywhere upward across the partitions. For $\alpha = +40°$, however, near the cavity corner the heat flux is downward. Close to the acute corner, the fluid is almost stagnant, achieving a higher temperature than the higher velocity fluid just below it, across the partition.

It is interesting to see that magnitudes of heat flux across the partitions for both inclinations, $\alpha = \pm 40$, appear uniform and almost identical, but greater than that of $\alpha = 0°$ throughout the main length of cavity

Table 2. Variation of η with aspect ratio, L/D, angle of inclination, α, and ratio of conductances, Rc (based on non-convective conduction only [13])

L/D	Rc	$\alpha = 0$	20	40	50
	0	0.4000	0.4064	0.4323	0.4629
5	1	0.4000	0.4290	0.5545	0.7130
	10	0.4000	0.4485	0.6578	0.9201
	100	0.4000	0.4525	0.6790	0.9628
	0	0.2000	0.2017	0.2084	0.2159
10	1	0.2000	0.2145	0.2742	0.3499
	10	0.2000	0.2242	0.3284	0.4594
	100	0.2000	0.2262	0.3395	0.4813
	0	0.1000	0.1003	0.1023	0.1042
20	1	0.1000	0.1068	0.1357	0.1733
	10	0.1000	0.1121	0.1642	0.2295
	100	0.1000	0.1131	0.1697	0.2406

Table 3. Nusselt numbers with variations of L/D, Pr, Gr, Rc and α

	Rc	$\alpha = -50$	-40	-20	0	20	40	50
L/D 10	0	1.046	1.251	1.885	3.783	8.163	13.533	15.402
Pr 0.72	1	1.279	1.426	1.897	3.048	5.389	7.244	7.096
Gr 2000	10	1.444	1.528	1.789	2.289	3.092	3.700	3.633
Ra 1440	100	1.463	1.524	1.728	2.101	2.696	3.152	3.129
L/D 10	0	1.191	1.531	3.578	17.439	32.722	34.664	37.878
Pr 0.72	1	1.690	2.101	4.347	14.833	25.591	23.303	19.194
Gr 10000	10	2.454	2.934	5.100	11.507	17.362	14.256	11.527
Ra 7200	100	2.607	3.160	5.206	13.124	21.230	18.334	14.674
L/D 20	0	1.027	1.361	3.635	19.143	36.948	41.907	44.666
Pr 4.0	1	1.664	3.110	4.590	16.599	29.964	28.401	24.554
Gr 2000	10	2.519	3.020	5.480	13.124	21.230	18.334	14.674
Ra 8000								
L/D 20	0	1.082	1.356	3.013	14.961	49.790	63.710	70.032
Pr 0.72	1	1.556	1.900	3.540	11.613	33.338	37.389	32.437
Gr 5000	10	2.109	2.421	3.726	7.979	17.263	19.388	17.500
Ra 3600	100	2.236	2.519	3.722	7.072	14.098	16.258	14.174

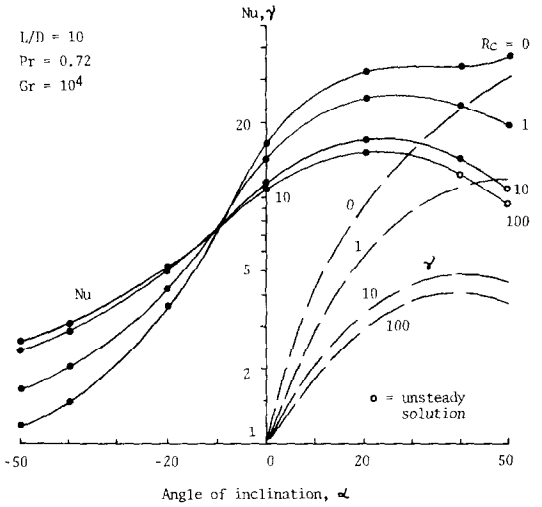

FIG. 3. Nusselt number, Nu, and the Nusselt number ratio, γ, as a function of Rc and α ($L/D = 10$, $Pr = 0.72$, $Gr = 10^4$).

except the cavity ends. Also, note that the heat flux crossing the partition wall is symmetric with respect to $x = l/2$.

Examination of the streamlines indicates that the basic number of eddies is one or two (Fig. 7). A flow regime with three or more eddies can arise during transition from a one- to a two-eddy pattern, or from a two- to a one-eddy pattern. The multi-eddy patterns appear to be unstable, and to evolve into the one- or two-eddy pattern. Two-eddy patterns appear at negative angles in general, whereas single eddies are present at positive angles. When L/D is large and Gr small, the convective eddy is weak with no discernible center of the eddy. In this case the convective flow is only in the axial direction, except in the end regime. With large value of Gr and L/D and $\alpha > 0$, the long, central streamlines appear weakly oscillating in the calculation. This rippling streamline was observed in an experiment with smoke [12]. A schematic presentation of these flow regimes in terms of streamline

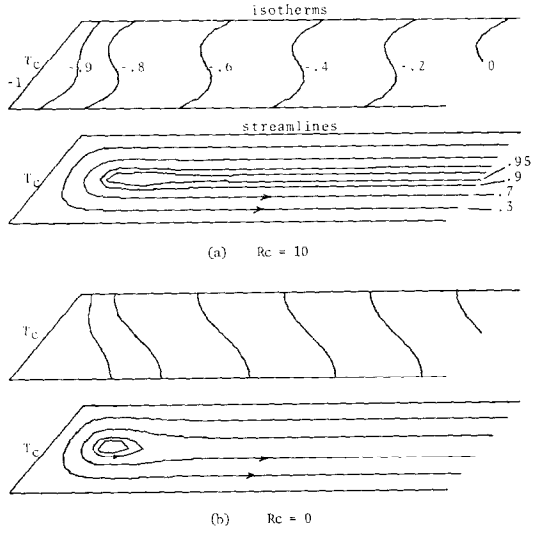

FIG. 4. Streamlines and isotherms ($L/D = 10$, $Pr = 0.72$, $Gr = 2000$, $\alpha = -40$).

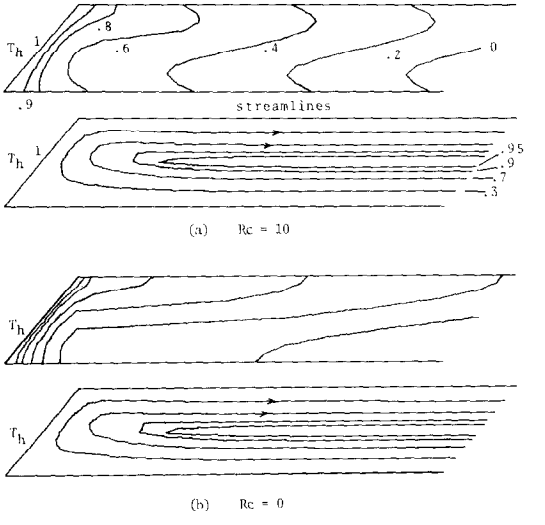

FIG. 5. Streamlines and isotherms ($L/D = 10$, $Pr = 0.72$, $Gr = 2000$, $\alpha = 40$).

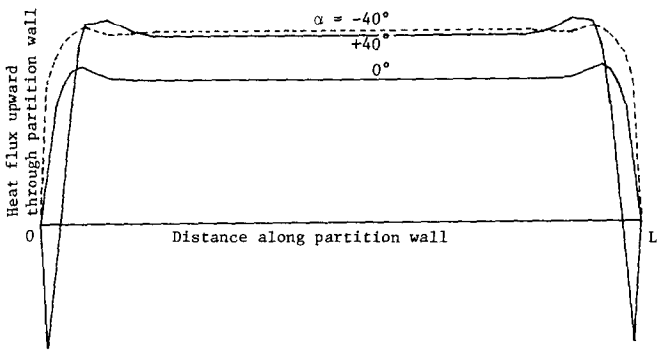

FIG. 6. Normalized heat flux across the tilted partition wall upward from the lower cavity ($L/D = 10$, $Rc = 10$).

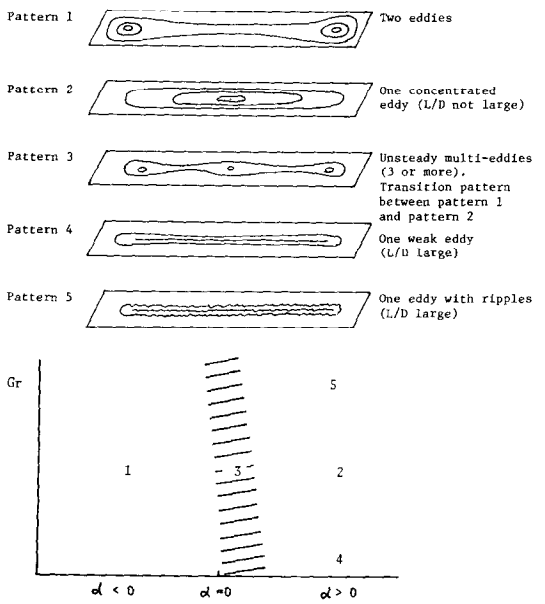

FIG. 7. Schematic flow patterns and their locations on Gr–α plane.

patterns is shown in Fig. 7. Rc influences the positions of eddies, but does not change the basic flow pattern.

The Nusselt number is not very sensitive to changes in the Prandtl number, for constant Rayleigh number. A few points were calculated, and the results shown in Table 4. Nu increases slightly with Pr for $\alpha > 0$, but stays almost constant for $\alpha < 0$. Examination of the plots of stream function and temperature for the points in Table 4 (plots not shown here) indicate that for a constant Rayleigh number there is an approximately inverse relation between Prandtl number and velocity, but little change in temperature with Prandtl number.

Catton *et al.* [8] included Nusselt number data for a single rectangular cavity of $L/D = 5$, with the long walls insulated. The analysis was based on the Galerkin method, with the Prandtl number assumed infinite. Their Rayleigh number was defined differently—when converted, their value of 1.8×10^6 becomes comparable to the $Pr = 20$, $Ra = 2880$ for data in Table 4. They obtained $Nu = 1.9$, 4.2, and 5.5 for $\alpha = -30$, 0, and $+20°$, in good agreement with the results presented here, except for the $+20°$ value, which is about a third lower.

Table 4. Ddpendence of Nusselt number on Prandtl number ($L/D = 5$)

L/D	Ra	Rc	Pr	$\alpha = -20$	$\alpha = 20$	$\alpha = 20$
5	2880	0	0.72	2.309	4.845	8.093
			4.0	2.312	4.935	8.591
			20.0	2.310	4.863	8.621
		10	0.72	2.890	3.340	4.287
			4.0	2.414	3.410	4.514
			20.0	2.402	3.345	4.538

One feature that turned up in this analysis is that for certain cases, solutions are of an unsteady nature, oscillating with constant amplitudes. Unsteady solutions occurred for cases with high Grashof numbers, large positive angles, and high Rc values. The three data points shown as open circles in Fig. 3 are averaged values of the Nusselt number for such oscillating flows. We suspect, for physical reasons, that these oscillations represent a real feature of the system rather than an artifact of the calculation procedure. More extensive numerical experiments on the unsteady-flow regime are underway in an attempt to resolve that question unambiguously.

Acknowledgement—Valuable comments made by Professor Kenneth N. Astill of Tufts University are gratefully acknowledged.

REFERENCES

1. G. K. Batchelor, Heat transfer by free convection across a closed cavity between vertical boundaries at different temperatures, *Q. appl. Math.* **12**, 209–233 (1954).
2. J. W. Elder, Laminar free convection in a vertical slot, *J. Fluid Mech.* **23**, 77–98 (1965).
3. E. R. G. Eckert and W. O. Carlson, Natural convection in an air layer enclosed between two vertical plates with different temperatures, *Int. J. Heat Mass Transfer* **2**, 106–120 (1961).
4. J. O. Wilkes and S. W. Churchill, The finite difference

computation of natural convection in a rectangular enclosure, *A.I.Ch.E. Jl* **12**, 161–166 (1966).
5. G. De Vahl Davis, Laminar natural convection in an enclosed rectangular cavity, *Int. J. Mass Transfer* **11**, 1675–1693 (1968).
6. C. Quon, High Rayleigh number convection in an enclosure. A numerical study, *Phys. Fluids* **15**, 12–19 (1972).
7. H. Ozoe, H. Sayama and S. W. Churchill, Natural convection in an inclined square channel, *Int. J. Heat Mass Transfer* **17**, 401–406 (1974).
8. I. Catton, P. S. Ayyasawamy and R. M. Clever, Natural convection flow in a finite, rectangular slot arbitrarily oriented with respect to the gravity vector, *Int. J. Heat Mass Transfer* **17**, 173 (1974).
9. D. Dropkin and E. Somerscales, Heat transfer by natural convection in liquids confined by two parallel plates which are inclined at various angles with respect to the horizontal, *J. Heat Transfer Trans. ASME* **92C**, 77–84 (1965).
10. J. N. Arnold, I. Catton and D. K. Edwards, Experimental investigation of natural convection in inclined rectangular regions of differing aspect ratios. ASME Paper 75-HT-62.
11. L. M. Trefethen, Natural convection inside inclined tubes. Paper 69-IC-189, Paris (1970).
12. L. M. Trefethen and K. C. Chung, The oneway heat wall—Analysis and experiments on a vertical stack of inclined cavities, *Proc. 6th Int. Heat Transfer Conf., Toronto* **4**, 119–124 (1978).
13. K. C. Chung and K. N. Astill, Heat conduction in a stack of parallelograms separated by thin partition walls. *J. Heat Transfer Trans. ASME* **99C**, 127–129 (1977).

CONVECTION NATURELLE DANS UN EMPILEMENT DE CAVITES INCLINEES ET EN FORME DE PARALLELOGRAMME

Résumé—On examine numériquement la convection naturelle dans un empilement vertical de cavités profondes, inclinées et en forme de parallélogramme. Une méthode explicite aux différences finies pour l'écoulement bidimensionnel est utilisée avec des conditions aux limites appropriées. Des nombres de Nusselt sont calculés pour différentes géométries, différents nombre de Prandtl, de Grashof et diverses conductances entre cavitées. Ces résultats analytiques fournissent une base de comparaison avec des mesures qui ont été obtenues avec des murs "à un seul passage". La procédure fournit aussi une base pour estimer le potentiel de telles structures à isolation asymétrique; une conclusion est que la conduction entre les cavités réduit considérablement l'asymétrie dans le nombre de Nusselt global.

FREIE KONVEKTION IN EINER SENKRECHTEN WAND AUS GESTAPELTEN SCHRÄGEN, PARALLELOGRAMMFÖRMIGEN ZELLEN

Zusammenfassung—Es wird die freie Konvektion innerhalb einer senkrechten Wand aus langen, schräg angeordneten, parallelogrammförmigen Zellen numerisch untersucht. Ein explizites finites Differenzenverfahren für zweidimensionale Strömung wurde mit den zugehörigen Randbedingungen formuliert. Nusselt-Zahlen werden für mehrere Geometrien, Prandtl-Zahlen, Grashof-Zahlen und Leitfähigkeiten zwischen den Hohlräumen berechnet. Diese analytischen Ergebnisse liefern eine Grundlage für Vergleiche mit Daten, die für in einer Richtung wärmeleitende Wände erzielt wurden. Das Verfahren liefert auch eine Grundlage für die Abschätzung der Leistungsfähigkeit solcher thermisch asymmetrischen Isolationsstrukturen. Ein Ergebnis ist, daß Leitung zwischen den Hohlräumen die erzielbare Asymmetrie der Wärmedurchgangszahl erheblich reduziert.

ЕСТЕСТВЕННАЯ КОНВЕКЦИЯ В ВЕРТИКАЛЬНОМ НАБОРЕ НАКЛОННЫХ ПОЛОСТЕЙ В ФОРМЕ ПАРАЛЛЕЛОГРАММОВ

Аннотация — Численно исследуется естественная конвекция внутри вертикального набора длинных наклонных полостей, имеющих форму параллелограммов. Сформулирована явная конечно-разностная схема для двухмерного потока вместе с соответствующими граничными условиями. Значения числа Нуссельта рассчитаны для различных геометрий, значений чисел Прандтля, Грасгофа и коэффициентов теплопроводности между полостями. Полученные результаты позволяют провести сравнение с данными по «односторонним» нагретым стенкам. Метод также позволяет провести оценку потенциальных возможностей использования таких несимметричных изолирующих структур; сделан вывод о том, что теплопроводность между полостями значительно уменьшает асимметрию в средних числах Нуссельта.